Non-Abelian statistics of Majorana zero modes in the presence of an Andreev bound state

Wenqin Chen,[1] Jiachen Wang,[1] Yijia Wu,[2] Junjie Qi,[3] Jie Liu,[1,*] and X. C. Xie[2,3,4]

[1]*School of Physics, Xi'an Jiaotong University, Ministry of Education Key Laboratory for Non-Equilibrium Synthesis and Modulation of Condensed Matter, Xi'an 710049, China*

[2]*International Center for Quantum Materials, School of Physics, Peking University, Beijing 100871, China*

[3]*Beijing Academy of Quantum Information Sciences, Beijing 100193, China*

[4]*CAS Center for Excellence in Topological Quantum Computation, University of Chinese Academy of Sciences, Beijing 100190, China*

(Received 7 May 2020; revised 24 January 2022; accepted 26 January 2022; published 9 February 2022)

Braiding Majorana zero modes (MZMs) is the key procedure toward topological quantum computation. We show such braiding can be well performed in a parallel semiconductor-superconductor nanowire structure. Considering the fact that the low-energy Andreev bound states (ABSs) usually mix with the MZMs in the present setup, we further investigate the braiding properties of MZMs when an ABS is presented. Our numerical simulation suggests that ABS can be regarded as a pair of weakly coupled MZMs. The dynamical hybridization of MZMs plus the non-Abelian braiding of MZMs would induce an arbitrary rotation on the Bloch sphere of a single qubit. Remarkably, such rotation is manipulable since the rotation parameters could be individually modulated. Thus, the dynamic evolution can be eliminated and the non-Abelian braiding statistics, independent of the braiding time, retrieves.

DOI: 10.1103/PhysRevB.105.054507

I. INTRODUCTION

A Majorana zero mode (MZM) is deemed as the most promising candidate for topological quantum computation (TQC) [1,2] for its non-Abelian statistics. The exploration for MZMs in topological superconductors (TSCs) has been drawing extensive attention in the last decade [3–12]. To date, TSCs have been realized in various experimental platforms [13–26]. The semiconductor-superconductor heterostructure, first experimentally realized one among these systems, is regarded as one of the most promising platforms to realize TQC. However, in spite of the promising signs, other complications such as the Andreev bound states (ABSs) still cannot be ruled out [27–37]. The ABS, which is viewed as a pair of fake MZMs, is widely observed in experiments and hard to get rid off in the present setup [30,32,33,37]. Though various experimental schemes have been proposed [30–33,38–48], there is still no convincing way to completely distinguish these two types of states.

The most likely way of distinguishing a MZM from the ABS is certainly based on its non-Abelian statistics [49–52]. However, only a few studies have paid attention to this topic thus far [53–55]. The main obstruction lies in two aspects. First, the braiding protocols which have been proposed so far are quite complicated and hard to realize experimentally [50,51]. Recently, a parallel structure was deemed as the most feasible way to achieve braiding operation [56–59]. However, the projective-measurement-based braiding in such a structure is not under control due to its probabilistic nature. Second, since the ABSs are hard to get rid off with state-of-art nanotechnology, it is necessary to study the braiding statistics in the presence of both MZMs and ABSs. Such investigation will also shed light on how to realize or modify TQC when an ABS is engaged.

This paper is motivated by attempting to solve the above two problems. First, we put forward a modified parallel structure [Fig. 1(d)] and show that the non-Abelian braiding of MZMs can be conveniently performed in such structure in a definite fashion. Second, we clarify the MZMs' braiding rule in the condition that one pair of MZMs is replaced by an ABS. Our braiding results suggest that an ABS can be decomposed into two weakly coupled MZMs. By combining the hybridization-induced evolution of the ABS and the non-Abelian braiding of the MZMs, a rotation to an arbitrary point on the single-qubit's Bloch sphere can be implemented. Such rotation is manipulable since each parameter can be individually modulated in the corresponding braiding section. In this way, the dynamic evolution can be eliminated and the non-Abelian braiding statistics, independent of the braiding time, retrieves. We conclude that though the presence of ABS creates complication, the non-Abelian braiding properties of the MZMs can still be observed.

II. MODIFIED TETRON STRUCTURE FOR NON-ABELIAN BRAIDING

Since the magnetic field can only be oriented along one direction, a parallel aligned structure tetron qubit is proposed for realizing the braiding through a series of projective measurements [53,56–58]. The tetron qubit consists of two parallel nanowires which are connected through a trivial superconductor. Hence the tetron qubit can be described by the Hamiltonian as $H_{\mathrm{T}} = \sum_i H_i + H_{\mathrm{S}} + H_{\mathrm{Tc}}$. Here H_i is the

*jieliuphy@xjtu.edu.cn

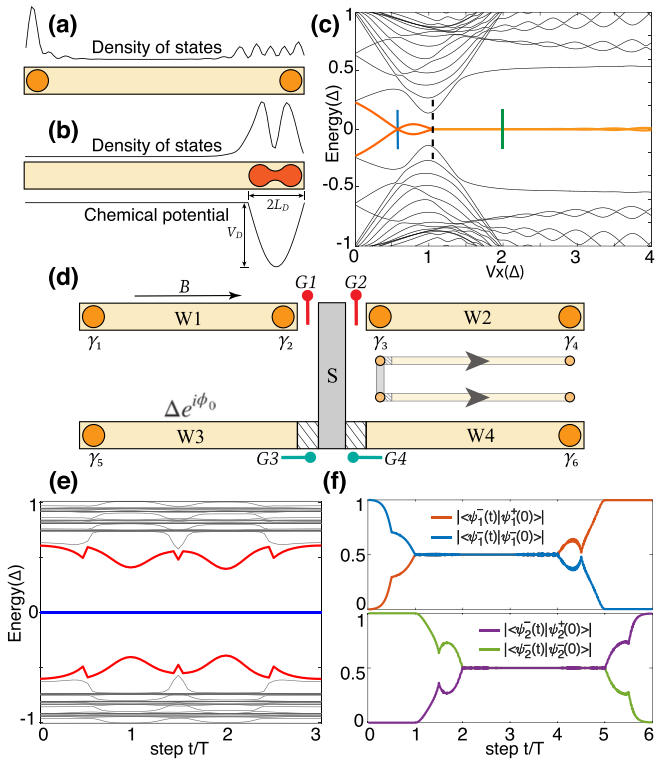

FIG. 1. (a) MZMs in a semiconductor-superconductor nanowire. (b) ABS in the same nanowire with a QD confinement presented. (c) The energy spectrum of the semiconductor-superconductor nanowire (with the QD confinement) versus the Zeeman energy. (d) The modified tetrom structure adopted for the braiding of the MZMs; the bottom nanowires ($W3, W4$) are ancillary ones during the braiding. All four arms are topologically nontrivial with $N_x = 100a$, $\mu = -2t_0$, and $V_x = 2\Delta$ [vertical green line in (c)]. The central region(S) is a trivial superconductor with length $N_c = 5a$, and other parameters are the same as those in the nanowires. (e) The energy spectrum of the system during the braiding with $\phi_0 = 0.5\pi$, in which the gap is always open. (f) Evolution of the wave function $\psi_j^-(t)$ during the braiding.

Hamiltonian for the ith nanowire whose explicit form is

$$\begin{aligned} H_i = & \sum\nolimits_{\mathbf{R},\mathbf{d},\alpha} -t_0(\psi^\dagger_{\mathbf{R}+\mathbf{d},\alpha}\psi_{\mathbf{R},\alpha} + \text{H.c.}) - \mu\psi^\dagger_{\mathbf{R},\alpha}\psi_{\mathbf{R},\alpha} \\ & + \sum\nolimits_{\mathbf{R},\mathbf{d},\alpha,\beta} -iU_R\psi^\dagger_{\mathbf{R}+\mathbf{d},\alpha}\hat{z}\cdot(\vec{\sigma}\times\mathbf{d})_{\alpha\beta}\psi_{\mathbf{R},\beta} \\ & + \sum\nolimits_{\mathbf{R},\alpha} \Delta e^{i\phi}\psi^\dagger_{\mathbf{R},\alpha}\psi^\dagger_{\mathbf{R},-\alpha} + \text{H.c.} \\ & + \sum\nolimits_{\mathbf{R},\alpha,\beta} \psi^\dagger_{\mathbf{R},\alpha}(V_x\vec{\sigma}_x)_{\alpha\beta}\psi_{\mathbf{R},\beta}, \end{aligned} \tag{1}$$

where $\mathbf{R}$ denotes the lattice site, $\mathbf{d}$ is the unit vector, α and β are the spin indices, t_0 denotes the hopping amplitude, μ is the chemical potential, U_R is the Rashba coupling strength, and V_x is the Zeeman energy. The superconducting pairing amplitude and the pairing phase are denoted as Δ and ϕ, respectively. In addition, H_S corresponds to the trivial superconductor which has the same form as H_i except for $U_R = 0$. H_{Tc} is the coupling term connecting the trivial superconductor and the four nanowires, which can be described by the Hamiltonian of

$$H_{Tc} = \sum\nolimits_{i,\mathbf{d},\alpha,\beta}[t_{ic}\psi^\dagger_{iNx(1),\alpha}\psi_{cN_c(1),\alpha} + \text{H.c.}]. \tag{2}$$

Note that the term $t_{ic}\psi^\dagger_{iNx(1),\alpha}\psi_{cN_c(1),\alpha}$ annihilates an electron at the right (N_x) or left end [Eq. (1)] of the ith nanowire ($i = 1, 2, 3, 4$) and creates an electron at the top [Eq. (1)] or bottom end (N_x) of the trivial superconductor. In other words, such a term describes the hopping between these two sites. The electron hopping strengths t_{ic} can be modulated by gates G_i as $t_{ic} = g_i t_0$ with $g_i = 0$ means disconnection with each other and $g_i = 1$ means perfectly connection with each other. The total parameters adopted here are specified referring to the experiment [13] as $\Delta = 250\ \mu$eV, $t_0 = 10\Delta$, and $U_R = 2\Delta$.

To remove the probabilistic nature of the projective measurement in the original tetron stucture, we propose a modified tetron structure as illustrated in Fig. 1(d), in which four additional gates ($G1 \sim G4$) are located near the intersection of the nanowires and the trivial superconductor. In such a structure, the braiding can be realized in a definite way through tuning the gate voltages in the corresponding gates [60,61]. Before the braiding, all four arms ($W1 \sim W4$) are topologically nontrivial, and gate voltages in $G1$ and $G2$ are turned on while in $G3$ and $G4$ are turned off, hence three pairs of MZMs (γ_{2j-1} and γ_{2j}, $j = 1, 2, 3$) are localized at the ends of the three divided sections. The braiding protocol takes three steps (the time cost for each step is T) to swap γ_2 and γ_3 spatially. In step 1, $G1$ is turned off and then $G3$ is turned on, hence γ_2 is teleported to $W3$. In step 2, $G2$ is turned off and then $G1$ is turned on, so γ_3 is teleported to the original position of γ_2. In step 3, $G3$ is turned off and then $G2$ is turned on. Consequently, the spatial positions of γ_2 and γ_3 are swapped.

To obtain the correct braiding results, the topological gap is required to remain open during the braiding. Therefore, a finite superconducting phase difference ϕ_0 should be kept between the top and bottom nanowires as shown below. If $\phi_0 = 0$, a domain wall (DW) structure [62] is formed when only $G2$ and $G3$ are turned off [the magnetic fields are pointed along one direction so the center region is twisted, see the inset of Fig. 1(d)]. In such a case, an additional pair of end modes which emerges from the bulk and collapses at the zero energy will ruin the braiding. On the contrary, when $\phi_0 \neq 0$, the DW structure is smoothed out so the gap remains open during the braiding [e.g., $\phi_0 = 0.5\pi$, see Fig. 1(e)] and the braiding results remain valid. In addition, the topological gap decreases exponentially with the increase of the length of the trivial superconductor N_c. Hence, it is better to choose N_c in the same order as the MZMs' coherence length. The latter is usually in the order of 10^2 nanometers and such length scale is feasible in the state-of-art technology.

With the topological gap kept open, our numerical simulation [Fig. 1(f)] confirms that the non-Abelian braiding can be accomplished in such a structure. The braiding of MZMs can be represented by the operator $B(\gamma_i, \gamma_j) = \exp(\frac{\pi}{4}\gamma_i\gamma_j)$, which transform the MZMs as $\gamma_i \to \gamma_j$ and $\gamma_j \to -\gamma_i$ [49]. The effective low-energy Hamiltonian describing the MZMs in each separated part of the tetron before braiding is in the form of $H_{j,\text{eff}} = i\epsilon_j\gamma_{2j-1}\gamma_{2j}$ ($j = 1, 2, 3$). Hence the eigenstates are in the wave functions of $\psi_j^\pm(0) = (\gamma_{2j-1} \pm i\gamma_{2j})/\sqrt{2}$. If γ_2 and γ_3 are swapped twice in succession, then the

wave function will evolve into $\psi_1^{\pm}(6T) = (\gamma_1 \mp i\gamma_2)/\sqrt{2} = \psi_1^{\mp}(0)$ and $\psi_2^{\pm}(6T) = (-\gamma_3 \pm i\gamma_4)/\sqrt{2} = -\psi_2^{\mp}(0)$. We simulate the wave-function evolution during the braiding as $|\psi_j^{\pm}(t)\rangle = U(t)|\psi_j^{\pm}(0)\rangle$, where $U(t) = \hat{T}\exp[i\int_0^t d\tau H(\tau)]$ is the time-evolution operator and $\hat{T}$ is the time-ordering operator [63–65]. The simulation results confirm that ψ_j^{+} evolves into ψ_j^{-} $(j = 1, 2)$ after adiabatically swapping γ_2 and γ_3 twice in succession, which demonstrate the non-Abelian braiding rules discussed above.

III. NON-ABELIAN BRAIDING IN THE PRESENCE OF ABS

We further investigate the braiding rule in the presence of an ABS. ABS is usually induced by the inhomogeneity at the interface, which can be modeled by a quantum dot (QD) confinement at the end of the nanowire [18,30,37]. As depicted in Fig. 1(b), a sinusoidal local chemical potential in the form of $V_d(R) = -V_D\cos(2\pi\frac{R-L_D}{2L_D})$ is presented at the right end of the nanowire, where $L_D = 10a$ is the half width of the QD and $V_D = 0.1t_0$ is the depth of the potential well. When an external magnetic field is applied, as shown in Fig. 1(c), a low-energy ABS will be trapped in the QD before the topological phase transition point. In contrast to the MZMs that distribute nonlocally at both ends [Fig. 1(a)], the ABS is a bound state localized at one end of the nanowire [Fig. 1(b)]. By replacing a pair of MZMs with an ABS in the modified tetron, distinctly different braiding results will be obtained. The final states after the same braiding process are time dependent and oscillate with the braiding time cost T, which is in stark contrast to the T-independent behavior of the braiding with true MZMs. As shown in Figs. 2(a)–2(c), $\psi_1^{-}(6T)$ is equal to $\psi_1^{+}(0)$ at $T = 400/\Delta$, and turns into a superposition of $\psi_1^{\pm}$ and $\psi_2^{\pm}$ at $T = 450/\Delta$, and then comes back to $\psi_1^{+}(0)$ at $T = 500/\Delta$.

The local density of states (LDOS) distribution in Figs. 2(d)–2(i) unveils the temporal and spatial profiles for both the ABS and the MZMs during the braiding. At the beginning, the LDOS of ABS exhibits a twin-peak structure, implying that the ABS can be treated as a pair of coupled MZMs γ_1 and γ_2, which are spatially separated with a finite distance. Such results are consistent with the previous studies [30,32,33]. From this point of view, the braiding in the presence of an ABS could be equivalent to the exchange between one free MZM and another MZM bounded in the ABS [66]. This feature can be further illustrated in Fig. 2(j) with the assistance of two ancillary MZMs γ_5' and γ_6'. In the initial stage, γ_5' and γ_6' are fused together due to the connection of the gates and would separate with each other if G3 and G4 are turned on. In this situation, the effective Hamiltonian can be described as

$$H_{\text{eff}}(t) = i\gamma_6'(\vec{\delta}\cdot\vec{\gamma}) + i\epsilon_d(t)\gamma_1\gamma_2. \tag{3}$$

Here $\vec{\gamma} = (\gamma_2, \gamma_3, \gamma_5')$ is defined as the Majorana vector and $\vec{\delta} = (t_1, t_2, t_3)$ is defined as the coupling vector, where t_1, t_2, t_3 are effective coupling strengths between γ_6' and $\gamma_2, \gamma_3, \gamma_5'$, respectively. If $\epsilon_d(t)$ keeps zero during the braiding process, $\vec{\delta}$ can be visualized as a radius vector in a 3D parameter space in analogy with the Bloch sphere shown in Fig. 2(k). Hence, the instantaneous eigenstates are MZM $\gamma_2 = \vec{\gamma}\cdot\hat{e}_\theta$, denoted as the vector along the polar direction (θ direction) perpendicular to $\vec{\delta}$, and MZM $\gamma_3 = \vec{\gamma}\cdot\hat{e}_\phi$, denoted as the vector along the polar direction (θ direction) perpendicular to $\vec{\delta}$. The braiding of MZMs can be represented by the operator $B(\gamma_2, \gamma_3) = \exp(\frac{\Omega_c}{2}\gamma_2\gamma_3)$ [67], where Ω_c is the solid angle spanned by the loop of $\vec{\delta}$ as shown in Fig. 2(k). While if $\epsilon_d(t)$ are not zero during the braiding process, since we braid the MZMs through ancillary MZM (γ_6'), as illustrated in Fig. 2(j), it can only couple to the half degree of the ABS's internal structure. From the effective Hamiltonian, we are able to distinguish two simultaneous processes of evolution, the geometric one and the dynamical one. Due to the first term of $H_{\text{eff}}(t)$, the geometric evolution of the instantaneous zero modes is that, as shown in Fig. 2(j), the bounded MZM $\gamma_2(\gamma_\theta)$ is moved out of ABS (splitting) in step 1, and the free MZM $\gamma_3(\gamma_\phi)$ is moved into the ABS (fusion, reversion of splitting) in step 2. Therefore, the geometric phase is still determined by the solid angle

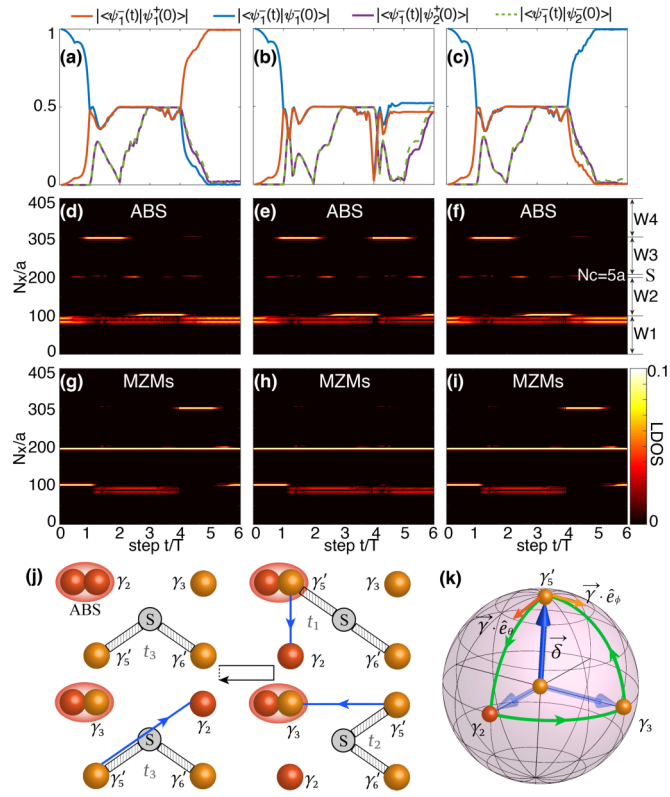

FIG. 2. Evolution of the wave function $\psi_1^{-} = (\gamma_1 - i\gamma_2)/\sqrt{2}$ with braiding time cost (a) $T = 400/\Delta$, (b) $T = 450/\Delta$, and (c) $T = 500/\Delta$. Here the Zeeman energy in the left arm ($W1$) is $V_x = 0.6\Delta$, hence the left arm is in the trivial regime with an ABS presented [see the blue vertical line in Fig. 1(c)]. All other parameters are the same as those in Fig. 1(d). (d)–(f) Evolution of the LDOS for ABS. The parameters correspond to (a)–(c), respectively. The MZMs are split and fused as indicated by the LDOS. (g)–(i) Corresponding evolution of the LDOS for MZMs. (j) A minimal sketch consisting of three MZMs and one ABS that shows the MZM can only couple to the half of ABS's internal structure. By manipulating the coupling strengths, MZMs can be moved out of and into the ABS due to geometric evolution. (k) The geometric path of the MZMs $\gamma_2 = \vec{\gamma}\cdot\hat{e}_\theta$ and $\gamma_3 = \vec{\gamma}\cdot\hat{e}_\phi$. A geometric phase is accumulated after a solid angle is spanned by the closed path of the coupling vector $\vec{\delta}$.

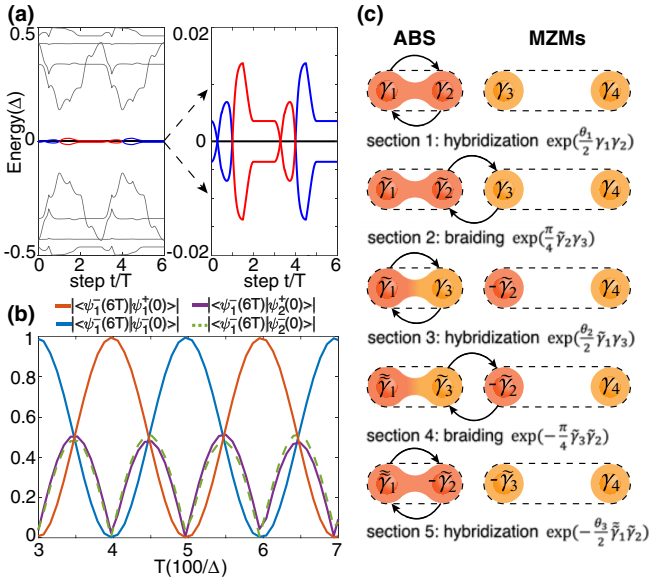

FIG. 3. (a) The eigenenergy of the ABS during the braiding. (b) Braiding results as functions of the braiding time cost T. (c) An illustration of the braiding process in the presence of an ABS. The whole braiding operation swapping γ_2 and γ_3 twice composes of five sections: Secs. 1, 3, and 5 are dynamical evolutions caused by the nonvanishing hybridization energy; Secs. 2 and 4 are non-Abelian braiding between two MZMs.

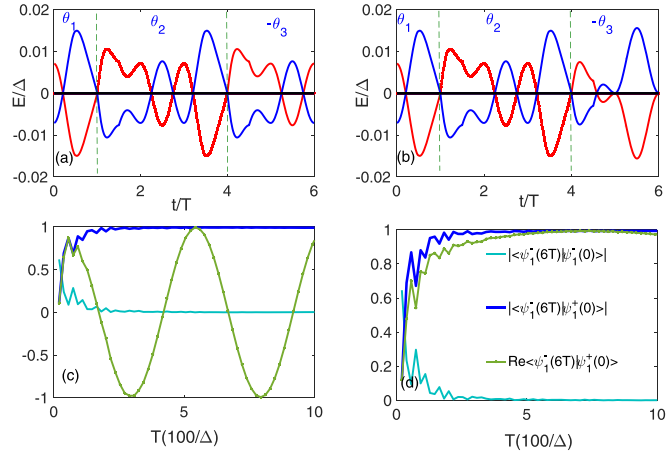

FIG. 4. (a) Energy spectrum of the ABS in the presence of a sinusoidal magnetic field $V_x = [0.59 + 0.02\cos(t/T \cdot \pi)]\Delta$ during the braiding. The other parameters are the same as those in Fig. 3. In this case, θ_2 vanishes since the integration of the eigenenergy cancels out. (b) Energy spectrum of the ABS with $V_x = [0.57 + 0.02\cos(t/T \cdot \pi)]\Delta$ during $t \in [4T, 6T]$, the other parameters are the same as (a). In this case, both θ_2 and $\theta_1 - \theta_3$ vanish. (c) The braiding results for (a), where the amplitude of $\psi_1^-(6T)$ is independent of T, while the phase of $\psi_1^-(6T)$ oscillates with T. (d) The braiding results for (b). Both the amplitude and the phase of $\psi_1^-(6T)$ are T independent, which retrieves the original robust non-Abelian braiding properties.

$\Omega_c = \pi$ spanned by the loop of $\vec{\delta}$ in Fig. 2(k). It should be very robust and insensitive to disorder or other perturbations, while the dynamical evolution would cause the hybridization of γ_1 and γ_2 in each step and induce the difference in splitting process.

For the first step ($t \in [0, T]$), as demonstrated in Fig. 3(a) [68], the hybridization happens between the two MZMs γ_1 and γ_2. The Hamiltonian for hybridization is $H_{\text{eff}}(t) = i\epsilon_1(t)\gamma_1\gamma_2$ and the corresponding evolution operator is $U_1 = e^{\frac{\theta_1}{2}\gamma_1\gamma_2}$, where $\frac{\theta_1}{2} = \int_0^T \epsilon_1(t)dt$ is the phase accumulated during the evolution. Such hybridization is equivalent to a unitary transformation on γ_1 and γ_2 [69]:

$$\tilde{\gamma}_1 = U_1^\dagger \gamma_1 U_1 = \cos(\theta_1)\gamma_1 + \sin(\theta_1)\gamma_2,$$
$$\tilde{\gamma}_2 = U_1^\dagger \gamma_2 U_1 = -\sin(\theta_1)\gamma_1 + \cos(\theta_1)\gamma_2. \quad (4)$$

At time $t = T$, $\tilde{\gamma}_2$ is fully separated from $\tilde{\gamma}_1$. After that, γ_3 starts to move into the ABS and hybridize with $\tilde{\gamma}_1$. In the meantime, $\tilde{\gamma}_2$ and γ_3 are swapped and the corresponding braiding operator is $B(\tilde{\gamma}_2, \gamma_3) = e^{\frac{\pi}{4}\tilde{\gamma}_2\gamma_3}$. The whole braiding operation can be decomposed into five braiding sections as sketched in Fig. 3(c). The evolution operator for such a whole braiding process can be expressed as the product of the evolution operator in each of these five steps as $U_F = e^{\frac{\theta_1}{2}\gamma_1\gamma_2} e^{\frac{\pi}{4}\tilde{\gamma}_2\gamma_3} e^{\frac{\theta_2}{2}\tilde{\gamma}_1\gamma_3} e^{\frac{\pi}{4}\tilde{\gamma}_2\tilde{\gamma}_3} e^{-\frac{\theta_3}{2}\tilde{\tilde{\gamma}}_1\tilde{\gamma}_2}$, where $\tilde{\tilde{\gamma}}_1 = e^{-\frac{\theta_2}{2}\tilde{\gamma}_1\gamma_3}\tilde{\gamma}_1 e^{\frac{\theta_2}{2}\tilde{\gamma}_1\gamma_3}$, $\tilde{\gamma}_3 = e^{-\frac{\theta_2}{2}\tilde{\gamma}_1\gamma_3}\gamma_3 e^{\frac{\theta_2}{2}\tilde{\gamma}_1\gamma_3}$, $\frac{\theta_2}{2} = \int_T^{4T} \epsilon_2(t)dt$, and $\frac{\theta_3}{2} = \int_{4T}^{6T} \epsilon_3(t)dt$ [70]. Therefore, in contrast to the MZMs' non-Abelian braiding, which merely depends on the topology, the braiding in the presence of an ABS is process dependent. Such braiding exhibits an accumulative behavior that the evolution in each step relies on the evolution result in the previous step. For instance, the state $\psi_1^-(0) = (\gamma_1 - i\gamma_2)/\sqrt{2}$ evolves into $\psi_1^-(6T) = (\tilde{\tilde{\gamma}}_1 + i\tilde{\gamma}_2)/\sqrt{2}$, in which both $\tilde{\tilde{\gamma}}_1 = e^{\frac{\theta_3}{2}\tilde{\tilde{\gamma}}_1\tilde{\gamma}_2}\tilde{\tilde{\gamma}}_1 e^{\frac{\theta_3}{2}\tilde{\tilde{\gamma}}_1\tilde{\gamma}_2}$ and $\tilde{\gamma}_2 = e^{\frac{\theta_3}{2}\tilde{\tilde{\gamma}}_1\tilde{\gamma}_2}\tilde{\gamma}_2 e^{-\frac{\theta_3}{2}\tilde{\tilde{\gamma}}_1\tilde{\gamma}_2}$ depend on the evolution in the previous step (the other states also show similar behaviors, see Ref. [71]). Hence, the weight of $\psi_1^-(6T)$ on $\psi_1^\mp(0)$ oscillates in a sinusoidal behavior as $[1 \mp \cos(\theta_2)]/2$, and on $\psi_2^\pm(0)$ oscillates as $\sin(\theta_2)/2$. The numerical results shown in Fig. 3(b) are fully consistent with the analytical prediction. Moreover, according to the peak positions and the oscillation period of $|\langle\psi_1^-(6T)|\psi_1^\pm(0)\rangle|$ [see Fig. 3(b)], it can be concluded that $\theta_2 = 2\pi T/\Delta T$. Remarkably, the explicit form of θ_2 suggests that the non-Abelian braiding properties of the MZMs can still be exhibited even when an ABS is involved. Specifically, $\theta_2 = 2\pi T/\Delta T$ indicates that $\psi_1^-(6T)$ will evolve into $\psi_1^+(0)$ if the dynamic phase can be eliminated, implying the presence of a geometric phase of π. In other words, if the geometric phase is absent, then the explicit form of θ_2 should be $\theta_2 = 2\pi(T/\Delta T + 1/2)$.

IV. MANIPULATING THE BRAIDING RESULTS

In the many-body basis ($|0\rangle$, $\Psi_1^\dagger|0\rangle$, $\Psi_2^\dagger|0\rangle$, $\Psi_1^\dagger\Psi_2^\dagger|0\rangle$), U_F has the matrix form of

$$i\begin{bmatrix} e^{i\frac{\theta_1+\theta_3}{2}}S_{\frac{\theta_2}{2}} & 0 & 0 & e^{i\frac{\theta_1-\theta_3}{2}}C_{\frac{\theta_2}{2}} \\ 0 & -e^{-i\frac{\theta_1+\theta_3}{2}}S_{\frac{\theta_2}{2}} & e^{-i\frac{\theta_1-\theta_3}{2}}C_{\frac{\theta_2}{2}} & 0 \\ 0 & e^{i\frac{\theta_1-\theta_3}{2}}C_{\frac{\theta_2}{2}} & -e^{i\frac{\theta_1+\theta_3}{2}}S_{\frac{\theta_2}{2}} & 0 \\ e^{-i\frac{\theta_1-\theta_3}{2}}C_{\frac{\theta_2}{2}} & 0 & 0 & e^{-i\frac{\theta_1+\theta_3}{2}}S_{\frac{\theta_2}{2}} \end{bmatrix}. \quad (5)$$

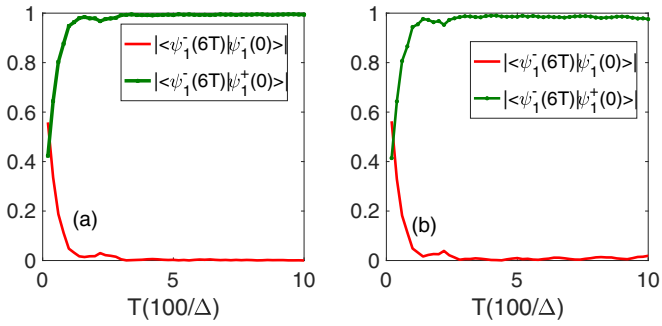

FIG. 5. The braiding results with different oscillation amplitudes of the weak sinusoidal magnetic field as (a) $V_x = [0.59 + 0.01\cos(t/T \cdot \pi)]\Delta$, and (b) $V_x = [0.59 + 0.03\cos(t/T \cdot \pi)]\Delta$. The comparison between (a) and (b) shows that the MZMs' braiding result is independent of the oscillation amplitude of the magnetic field, provided that the adiabatic condition is satisfied as $T \gtrsim 200/\Delta$.

where $S_{\frac{\theta_2}{2}} \equiv \sin(\theta_2/2)$ and $C_{\frac{\theta_2}{2}} \equiv \cos(\theta_2/2)$. This off-diagonal form of the braiding matrix demonstrates the non-Abelian nature of the braiding operation. Moreover, by tuning θ_2 and θ_3, the corresponding qubit can be rotated into any point on the Bloch sphere by such a braiding operation, which is beyond the MZM-based braiding operation. Specifically, the polar angle θ_2 is the dynamic phase accumulated during $t \in [T, 4T]$, and the azimuthal angle $\theta_1 \pm \theta_3$ is determined by the period $t \in [0, T]$ and $t \in [4T, 6T]$. Both these phases can be modulated individually by tuning the parameters in the corresponding braiding sections.

The manipulation of such phase angles can be assisted by combining the technology in geometric quantum computation (GQC) [72–75]. In GQC, the dynamic phase can be eliminated through the spin-echo technique which reverses the sign of the eigenenergy at the middle of the symmetric braiding protocol. Noticing that the spectrum of the ABS [Fig. 1(c)] crosses the zero energy in the vicinity of $V_x = 0.6\Delta$. Hence, it is possible to reverse the ABS's eigenenergy by modulating the Zeeman energy. For instance, by applying a sinusoidal magnetic field $V_x = [V_{x0} + V_{x1}\cos(t\pi/T)]$, the eigenenergy will cross the zero energy during the braiding. In such a situation, the oscillation period will increase tenfold since the dynamic phase is nearly eliminated. In the special case of $V_{x0} = 0.59\Delta$ and $V_{x1} = 0.02\Delta$, as shown in Fig. 4(a), the dynamic phase θ_2 can be completely canceled out (actually, θ_2 is also canceled out if $V_{x1} = 0.01\Delta$, indicating V_{x1} does not need fine-tuning), so the braiding result $\psi_j^+ \to \psi_j^-$ independent of the braiding time cost T retrieves [Fig. 4(c)]. However, since the azimuthal angle $\theta_1 - \theta_3$ does not vanish, $\mathrm{Re}\langle\psi_1^+(6T)|\psi_1^-(0)\rangle$ still oscillates with T. Considering the fact that the modulation could be individually performed in each braiding section, by tuning $V_{x0} = 0.570\Delta$ during $t \in [4T, 6T]$ while keeping the other parameters invariant, $\theta_1 - \theta_3$ can also be eliminated. Therefore, the non-Abelian braiding recovers the T-independent form [Fig. 4(d)] as in the case that only MZMs are involved.

We also find that the braiding results are insensitive to the oscillation amplitude of such a sinusoidal magnetic field. For instance, Fig. 5 shows the braiding results with respect to the braiding time cost T in the conditions of $V_x = 0.59 + 0.01\cos(t\pi/T)]\Delta$ [see Fig. 5(a)] and $V_x = 0.59 + 0.03\cos(t\pi/T)]\Delta$ [see Fig. 5(b)], respectively. It can be seen that the non-Abelian statistics is well preserved for different oscillation amplitudes of the magnetic field, which implies that imposing such an additional magnetic field is an efficient way to eliminate the dynamic phase.

V. DISCUSSION

We have shown that the non-Abelian braiding of MZMs can be well performed in a modified tetron structure. Furthermore, we also investigate the MZMs' braiding properties when a low-energy ABS is presented. Although we have not discussed the noise effect induced by the ABS [76,77], we can rationally expect that its influence is quite small, since the previous studies indicate that the spin-echo techniques can largely reduce the noise effect [75]. Finally, we want to point out that the phase elimination method discussed above can also be performed for the finite-size-effect-induced partially overlapped MZMs since the ABS is deemed as a pair of weakly coupled MZMs with finite separation. In one of our previous works [39], we revealed that the spectrum of such partially overlapped MZMs will cross at zero energy with definite parity by modulating the Zeeman field or the gate voltage. It implies that the dynamic evolution can be well manipulated by modulating either the Zeeman field or the gate voltage. Therefore, the TQC can be realized in a shorter TSC nanowire, which possesses advantages such as supporting universal gate operation through modulating the dynamical evolution.

ACKNOWLEDGMENTS

W. Chen and J. Wang contributed equally to this paper. This paper is financially supported by National Natural Science Foundation of China (Grant No. 11974271) and National Basic Research Program of China (Grants No. 2017YFA0303301 and No. 2019YFA0308403).

[1] A. Kitaev, Phys. Usp. **44**, 131 (2000).
[2] C. Nayak, S. H. Simon, A. Stern, M. Freedman, S. Das Sarma, Rev. Mod. Phys. **80**, 1083 (2008).
[3] L. Fu and C. L. Kane, Phys. Rev. Lett. **100**, 096407 (2008).
[4] J. D. Sau, R. M. Lutchyn, S. Tewari, S. Das Sarma, Phys. Rev. Lett. **104**, 040502 (2010).
[5] S. Fujimoto, Phys. Rev. B. **77**, 220501(R) (2008).
[6] M. Sato, Y. Takahashi, and S. Fujimoto, Phys. Rev. B **82**, 134521 (2010).
[7] J. Alicea, Phys. Rev. B **81**, 125318 (2010).
[8] R. M. Lutchyn, J. D. Sau, and S. Das Sarma, Phys. Rev. Lett. **105**, 077001 (2010).
[9] Y. Oreg, G. Refael, and F. von Oppen, Phys. Rev. Lett. **105**, 177002 (2010).
[10] A. C. Potter and P. A. Lee, Phys. Rev. B **83**, 094525 (2011).

[11] M. Hell, M. Leijnse, and K. Flensberg, Phys. Rev. Lett. **118**, 107701 (2017).

[12] F. Pientka, A. Keselman, E. Berg, A. Yacoby, A. Stern, and B. I. Halperin, Phys. Rev. X **7**, 021032 (2017).

[13] V. Mourik, K. Zuo, S. M. Frolov, S. R. Plissard, E. P. A. M. Bakkers, L. P. Kouwenhoven, Science **336**, 1003 (2012).

[14] M. T. Deng, C. L. Yu, G. Y. Huang, M. Larsson, P. Caroff, and H. Q. Xu, Nano Lett. **12**, 6414 (2012).

[15] A. Das, Y. Ronen, Y. Most, Y. Oreg, M. Heiblum, and H. Shtrikman, Nat. Phys. **8**, 887 (2012).

[16] Ö. Gül, H. Zhang, J. D. S. Bommer, M. W. A. de Moor, D. Car, S. R. Plissard,E. P. A. M. Bakkers, A. Geresdi, K. Watanabe, T. Taniguchi, L. P. Kouwenhoven, Nat. Nanotechnol. **13**, 192 (2018).

[17] H. Zhang, C.-X. Liu, S. Gazibegovic, D. Xu, J. A. Logan, G. Wang, N. van Loo, Jouri D. S. Bommer, M. W. A. de Moor, D. Car, R. L. M. Op het Veld, P. J. van Veldhoven, S. Koelling, Marcel A. Verheijen, M. Pendharkar, Daniel J. Pennachio, B. Shojaei, J. Sue Lee, C. J. Palmstrom, E. P. A. M. Bakkers, S. Das Sarma, Leo P. Kouwenhoven, Nature (London) **556**, 74 (2018).

[18] S. M. Albrecht, A. P. Higginbotham, M. Madsen, F. Kuemmeth, T. S. Jespersen, J. Nygard, P. Krogstrup, and C. M. Marcus, Nature (London) **531**, 206 (2016).

[19] S. Nadj-perge, l. K. Drozdov, J. Li, H. Chen, S. Jeon, J. Seo, Allan H. MacDonald B. A. Bernevig, A. Yazdani, Science **346**, 602 (2014).

[20] B. E. Feldman, M. T. Randeria, J. Li, S. Jeon, Y. Xie, Z. Wang, Ilya K. Drozdov, B. A. Bernevig, and A. Yazdani, Nat. Phys. **13**, 286 (2017).

[21] H. H. Sun, K. W. Zhang, L. H. Hu, C. Li, G. Y. Wang, H. Y. Ma, Z. A. Xu, C. L. Gao, D. D. Guan, Y. Y. Li, C. Liu, D. Qian, Y. Zhou, L. Fu, S. C. Li, F. C. Zhang, and J. F. Jia, Phys. Rev. Lett. **116**, 257003 (2016).

[22] D. Wang, L. Kong, P. Fan, H. Chen, S. Zhu, W. Liu, L. Cao, Y. Sun, S. Du, J. Schneeloch, R. Zhong, G. Gu, L. Fu, H. Ding, and H.-J. Gao, Science **362**, 333 (2018).

[23] Q. Liu, C. Chen, T. Zhang, R. Peng, Y. J. Yan, Chen-Hao-Ping Wen, X. Lou, Y. L. Huang, J. P. Tian, X. L. Dong, G. W. Wang, W. C. Bao, Q. H. Wang, Z. P. Yin, Z. X. Zhao, and D. L. Feng, Phys. Rev. X **8**, 041056 (2018).

[24] P. Zhang, K. Yaji, T. Hashimoto, Y. Ota, T. Kondo, K. Okazaki, Z. Wang, J. Wen, G. D. Gu, H. Ding, and S. Shin, Science **360**, 182 (2018).

[25] A. Fornieri, Alexander M. Whiticar, F. Setiawan, E. Portolés, Asbjørn C. C. Drachmann, A. Keselman, S. Gronin, C. Thomas, T. Wang, R. Kallaher, Geoffrey C. Gardner, E. Berg, Michael J. Manfra, A. Stern, Charles M. Marcus, and F. Nichele, Nature (London) **569**, 89 (2019).

[26] H. Ren, F. Pientka, S. Hart, A. Pierce, M. Kosowsky, L. Lunczer, R. Schlereth, B. Scharf, E. M. Hankiewicz, L. W. Molenkamp, B. I. Halperin, and A. Yacoby, Nature (London) **569**, 93 (2019).

[27] J. Liu, Andrew C. Potter, K. T. Law, and Patrick A. Lee, Phys. Rev. Lett. **109**, 267002 (2012).

[28] G. Kells, D. Meidan, and P. W. Brouwer, Phys. Rev. B **86**, 100503(R) (2012).

[29] E. Prada, P. San-Jose, and R. Aguado, Phys. Rev. B **86**, 180503(R) (2012).

[30] C.-X. Liu, Jay D. Sau, and S. D. Sarma, Phys. Rev. B **97**, 214502 (2018).

[31] C. Moore, T. D. Stanescu, and S. Tewari, Phys. Rev. B **97**, 165302 (2018).

[32] A. Vuik, B. Nijholt, A. R. Akhmerov, and M. Wimmer, SciPost Phys. **7**, 061 (2019).

[33] F. Penaranda, R. Aguado, P. San-Jose, and E. Prada, Phys. Rev. B **98**, 235406 (2018).

[34] C. Reeg, O. Dmytruk, D. Chevallier, D. Loss, and J. Klinovaja, Phys. Rev. B **98**, 245407 (2018).

[35] T. D. Stanescu and S. Tewari, Phys. Rev. B **100**, 155429 (2019).

[36] A. Grivnin, E. Bor, M. Heiblum, Y. Oreg, and H. Shtrikman, arXiv:1807.06632.

[37] C. Fleckenstein, F. Dominguez, N. T. Ziani, and B. Trauzettel, Phys. Rev. B **97**, 155425 (2018).

[38] R. V. Mishmash, D. Aasen, A. P. Higginbotham, and J. Alicea, Phys. Rev. B **93**, 245404 (2016).

[39] J. Liu, J. Song, Q.-F. Sun, and X. C. Xie, Phys. Rev. B **96**, 195307 (2017).

[40] T. O. Rosdahl, A. Vuik, M. Kjaergaard, and A. R. Akhmerov, Phys. Rev. B **97**, 045421 (2018).

[41] J. Cayao, E. Prada, P. San-Jose, and R. Aguado, Phys. Rev. B **91**, 024514 (2015).

[42] G. C. Menard, G. L. R. Anselmetti, E. A. Martinez, D. Puglia, F. K. Malinowski, J. S. Lee, S. Choi, M. Pendharkar, C. J. Palmstrom, K. Flensberg, C. M. Marcus, L. Casparis, and A. P. Higginbotham, Phys. Rev. Lett. **124**, 036802 (2020).

[43] H. Zhang, D. E. Liu, M. Wimmer, and L. P. Kouwenhoven, Nat. Commun. **10**, 5128 (2019).

[44] K. Yavilberg, E. Ginossar, and E. Grosfeld, Phys. Rev. B **100**, 241408(R) (2019).

[45] A. Ptok, A. Kobialka, and T. Domanski, Phys. Rev. B **96**, 195430 (2017).

[46] Oladunjoye A. Awoga, J. Cayao, and Annica M. Black-Schaffer, Phys. Rev. Lett. **123**, 117001 (2019).

[47] J. Cayao, P. San-Jose, A. M. Black-Schaffer, R. Aguado, and E. Prada, Phys. Rev. B **96**, 205425 (2017).

[48] J. Cayao and A. M. Black-Schaffer, Eur. Phys. J. Spec. Top. **227**, 1387 (2018).

[49] D. A. Ivanov, Phys. Rev. Lett. **86**, 268 (2001).

[50] J. Alicea, Y. Oreg, G. Refael, F. von Oppen, and M. P. A. Fisher, Nat. Phys. **7**, 412 (2011).

[51] B. van Heck, A. R. Akhmerov, F. Hassler, M. Burrello, and C. W. J. Beenakker, New J. Phys. **14**, 035019 (2012).

[52] D. Aasen, M. Hell, R. V. Mishmash, A. Higginbotham, J. Danon, M. Leijnse, T. S. Jespersen, J. A. Folk, C. M. Marcus, K. Flensberg, and J. Alicea, Phys. Rev. X **6**, 031016 (2016)

[53] R. V. Mishmash, B. Bauer, F. von Oppen, and J. Alicea, Phys. Rev. B **101**, 075404 (2020).

[54] I. C. Fulga, B. van Heck, M. Burrello, and T. Hyart, Phys. Rev. B **88**, 155435 (2013).

[55] J. Manousakis, C. Wille, A. Altland, R. Egger, K. Flensberg, and F. Hassler, Phys. Rev. Lett. **124**, 096801 (2020).

[56] S. Vijay and L. Fu, Phys. Rev. B **94**, 235446 (2016).

[57] T. Karzig, C. Knapp, R. M. Lutchyn, P. Bonderson, M. B. Hastings, C. Nayak, J. Alicea, K. Flensberg, S. Plugge, Y. Oreg, C. M. Marcus, and M. H. Freedman, Phys. Rev. B **95**, 235305 (2017).

[58] C. Schrade and L. Fu, Phys. Rev. Lett. **121**, 267002 (2018).

[59] Y. Oreg and F. von Oppen, Ann. Rev. Condens. Matter Phys. **11**, 397 (2020).

[60] C. S. Amorim, K. Ebihara, A. Yamakage, Y. Tanaka, and M. Sato, Phys. Rev. B **91**, 174305 (2015).
[61] F. Harper, A. Pushp, and R. Roy, Phys. Rev. Research **1**, 033207 (2019).
[62] X. Liu, X. Li, D.-L. Deng, X.-J. Liu, S. Das Sarma, Phys. Rev. B **94**, 014511 (2016).
[63] D. Sun and J. Liu, Phys. Rev. B **97**, 035311 (2018).
[64] Y. Wu, H. Liu, J. Liu, H. Jiang, and X. C. Xie, Natl. Sci. Rev. **7**, 572 (2019).
[65] Y. Wu, H. Jiang, J. Liu, H. Liu, and X. C. Xie, Phys. Rev. Lett. **125**, 036801 (2020).
[66] Here the hybridization of the MZMs can be observed through the LDOS. More information can be found in the Supplemental Material at http://link.aps.org/supplemental/10.1103/PhysRevB.105.054507.
[67] J. Liu, W. Chen, M. Gong, Y. Wu, and X. C. Xie, Sci. China-Phys. Mech. and Astron. **64**, 117811 (2021).
[68] Even though the initial energy of ABS is very small, the hybridization energy induced by the splitting and fusion process of MZMs are usually on the order of $10^{-}2\Delta$.
[69] Y.-F. Zhou, Z. Hou, and Q.-F. Sun, Phys. Rev. B **99**, 195137 (2019).
[70] Here ϵ_2 is induced by the hybridization between $\tilde{\gamma}_1$ and γ_3, while ϵ_3 is induced by the hybridization between $\tilde{\tilde{\gamma}}_1$ and $-\tilde{\gamma}_2$.
[71] We can conclude that the new rule of MZMs evolves as $\gamma_3 \to -\tilde{\gamma}_3$ and $\gamma_2 \to -\tilde{\tilde{\gamma}}_2$, for more information see Supplemental Material at http://link.aps.org/supplemental/10.1103/PhysRevB.105.054507.
[72] A. A. Abdumalikov, J. M. Fink, K. Juliusson, M. Pechal, S. Berger, A. Wallraff, and S. Filipp, Nature (London) **496**, 482 (2013).
[73] T. Yan, B.-J. Liu, K. Xu, C. Song, S. Liu, Z. Zhang, H. Deng, Z. Yan, H. Rong, K. Huang, M.-H. Yung, Y. Chen, and D. Yu, Phys. Rev. Lett. **122**, 080501 (2019).
[74] B.-J. Liu, X.-K. Song, Z.-Y. Xue, X. Wang, and M.-H. Yung, Phys. Rev. Lett. **123**, 100501 (2019).
[75] T. Karzig, Y. Oreg, G. Refael, and M. H. Freedman, Phys. Rev. X **6**, 031019 (2016).
[76] C. Knapp, T. Karzig, Roman M Lutchyn, C. Nayak, Phys. Rev. B **97**, 125404 (2018).
[77] A. Khindanov, D. Pikulin, and T. Karzig, SciPost Phys. **10**, 127 (2021).